Journal of Physics D: Applied Physics

Check for updates

OPEN ACCESS

RECEIVED
8 September 2026

REVISED
3 October 2026

ACCEPTED FOR PUBLICATION
15 October 2026

PUBLISHED
5 November 2026

Original content from this work may be used under the terms of the Creative Commons Attribution 4.0 licence.

Any further distribution of this work must maintain attribution to the author(s) and the title of the work, journal citation and DOI.

PAPER

Consequences of tilt of the magnetic field in magnetically enhanced capacitively coupled plasma reactors

Mark J Kushner*

University of Michigan, Electrical Engineering and Computer Science, 1301 Beal Ave, Ann Arbor, MI, 48109-2122, United States of America

* Author to whom any correspondence should be addressed.

E-mail: mjkush@umich.edu

Keywords: capacitively coupled plasma, magnetically enhanced, plasma simulation, digital twin

Abstract

Magnetically enhanced reactive ion etching (MERIE) reactors are capacitively coupled plasmas (CCPs) used in microelectronic fabrication with a static magnetic field that is typically parallel to the wafer. The purpose of the magnetic field is to increase plasma density and ion fluxes, while affording some control to the ion energy and angular distribution (IEAD) incident onto the wafer. The uniformity of the plasma produced reactive fluxes onto the wafer are sensitive to the orientation of the magnetic field with respect to the wafer. For example, fluxes are sensitive to the tilt of the magnetic field with respect to the surface of the wafer, as opposed to being strictly parallel to the wafer. There is some likelihood that this angle may change from before to after preventative maintenance of a commercial MERIE reactor. In this paper, we discuss results from a computational investigation of the consequences of tilt in the magnetic field in MERIE reactors on the uniformity of ion fluxes and IEADs delivered to the wafer. This investigation was performed for CCPs sustained in Ar and Ar/Cl_2 mixtures at tens of mTorr pressure with magnetic fields up to 150 G. We found that tilt of the magnetic field of as small as 1° produces significant side-to-side non-uniformity in ion fluxes delivered across a 20 cm wafer. There is less sensitivity of the IEAD to the tilt angle. The dynamics of electric field reversals (EFRs), which are common in MERIE reactors, are sensitive to the tilt angle, with the EFRs traversing diagonally across the reactor as the tilt angle increases. The role of digital twins in insuring consistent performance of plasma reactors is discussed.

1. Introduction

Plasma etching for microelectronics fabrication requires fine control of the magnitude of ion fluxes and their energy and angular distributions onto the wafer [1]. Magnetically enhanced reactive ion etching (MERIE) reactors are capacitively coupled plasmas (CCPs) which have an externally applied static magnetic field which is ideally parallel to the surface of the wafer [2–8]. MERIE reactors provide an additional degree of control over plasma properties and reactive fluxes to the substrate. MERIE reactors were among the first commercial plasma etching tools deployed in high volume manufacturing (HVM) [7, 8]. Although applications requiring high aspect ratio etching benefit from high energy ions [1], the renewed interest in MERIEs results, in part, from the ability to control and lower the energy of ions incident onto the wafer [9], as might be needed for atomic scale processing such as atomic layer etching [10]. Magnetic fields parallel to the substrate may result in electric field reversals (EFRs) in which the electric field approaching the sheath is oriented to accelerate electrons into the wafer with a narrow angular distribution [11]. Electron fluxes having these energy and angular distributions are able to better remediate positive charging of features. There have also been several investigations of CCPs having magnetics fields perpendicular to the wafer with the goal of increasing plasma density and uniformity [12, 13]

The magnitude of the magnetic field parallel to the substrate in MERIEs, typically up to a few hundred Gauss, is large enough to strongly magnetize the electrons while weakly magnetizing the ions. The

© 2026 The Author(s). Published by IOP Publishing Ltd

purpose of the magnetic field is several-fold. The rate of loss of electrons to the surfaces is reduced by the magnetic field, thereby increasing plasma density for a given power deposition. With a reduction of mobility of electrons perpendicular to the substrate, the sheath potential is reduced and, in some cases, an EFR can occur in the pre-sheath and into the sheath. For large magnetic fields, the bulk plasma becomes resistive and sustains a significant voltage drop, a phenomenon typically not observed in conventional CCPs [11]. A direct consequence of the reduction in sheath voltage and the EFR is a reduction in the ion energies incident onto the wafer [9, 11]. Ions striking the substrate produce secondary electrons which are accelerated by the sheath electric field back into the plasma, producing significant ionization and excitation. The range of these secondary electrons is reduced by their cyclotron motion about the parallel magnetic field lines, thereby localizing ionization by secondary electrons close to the substrate. All of these magnetic field dependent processes can be leveraged to customize reactive fluxes to the substrate.

In HVM of microelectronics devices, uniformity of ion fluxes to the wafer is of paramount importance [1]. In HVM, preventative maintenance (PM) of plasma reactors is performed on a periodic basis that often requires some disassembly of the reactor to replace consumable parts or to clean the reactor. Upon reassembly, the original configuration and dimensional tolerances should be exactly restored. The magnetic field in MERIEs is typically produced by solenoidal coils [6–8]. Re-assembly of the reactor during PM then requires that the alignment of the solenoidal coils and the substrate be precise to provide a magnetic field that is again parallel to the substrate. Deviations of the magnetic field from being parallel to the substrate (here called a *tilt*) would potentially lead to non-uniformities in reactant fluxes and process variability between different plasma reactors following PM.

Development of digital twins (DTs) for plasma reactors used in HVM microelectronics fabrication is a leading topic in the field. The format of many current DTs are surrogate models (SMs) in which computed data from physics models are used to train machine learning representations of the plasma reactor—SMs [1, 14–18]. The use of SMs for real time control and, for example, optimization of reactant fluxes to the wafer for a given chemistry over a limited range of conditions is already finding applications in HVM. However, use of SMs for development of new processes using new chemistries will continue to be a challenge. These challenges result from two primary causes. The first is the sometimes sparse availability of fundamental data (i.e. cross sections, reactions mechanisms, surface reaction probabilities) needed by the physics models. The second is the vast parameter space of possible operating conditions needed to be covered by the physics models for training the SM—power, pulsing, frequencies, mixtures, pressures, temperatures, reactor geometries, inductive-vs-capacitive coupling, voltage-waveform tailoring. A SM that addresses these vast parameters spaces and so covers all design possibilities could be termed the *omni-surrogate-model*. For the foreseeable future, the *omni-surrogate-model* may be elusive due to these challenges.

Given the difficulty of developing a *omni-surrogate-model*, DTs based on SMs in the near future may be best applied to more finite problems over small parameter spaces for which exhaustive and comprehensive training data can be produced by physics models. Restoring a plasma reactor to its previous state following preventative maintenance represents fertile ground for SMs to make impact in HVM. When disassembling, maintaining and reassembling a plasma reactor, there are, in principle, a finite number of variations between the *before-and-after* configurations of the reactor. These finite number of variations are amenable to physics models being able to produce the data required to train the SMs. Using appropriate sensors, SMs can then quickly isolate the difference(s) in the *before-and-after* configurations that might be responsible for the reactor not reproducing prior behaviour.

In this paper, results from a computational investigation of MERIEs are discussed in which the magnetic field deviates from being parallel to the substrate. The purpose of this investigation is to assess the impact of the tilt of the magnetic field on the uniformity of ion fluxes, and the uniformity ion energy and angular distributions (IEADs) to the wafer. The outcome of calculations of this type are, in principle, the training data required for SMs that can be used to assess and correct the reactor configurations to insure that *before-and-after* maintenance the reactor produces the same result. The investigation was performed for a MERIE sized for a 20 cm wafer sustained in argon and Ar/Cl_2 mixtures at a pressure of 40 mTorr. Although the results are likely sensitive to the details of the molecular and attaching chemistries used in plasma etching, this investigation was performed in argon and simple gas mixtures to focus the discussion on the plasma transport issues.

The model used in this investigation is described in section 2. Plasma properties for MERIEs having tilted magnetic fields in Ar and Ar/Cl_2 mixtures, and the sensitivity to anomalous diffusion are discussed in section 3. Concluding remarks are in section 4.

2. Description of the model

The model used in this investigation is Hybrid Plasma Equipment Model (HPEM), described in detail in [19–21]. The HPEM is a modular, 2-dimensional multi-fluid plasma hydrodynamics model that incorporates both continuum and particle kinetic techniques. In this investigation the HPEM modules used are the Electron Monte Carlo Simulation (eMCS), the Fluid-Kinetics Poisson Module and the Plasma Chemistry Monte Carlo Module. With the exception of updates to the anomalous transport algorithms, this implementation of the HPEM in a magnetized low pressure reactor is essentially the same as described in [21]. A brief overview is provided.

Continuity, momentum and energy equations are integrated on a 2-dimensional structured Cartesian mesh for each heavy particle species (ions and neutrals). Transport of bulk electrons is addressed using a drift-diffusion formulation with tensor transport coefficients. Rate and transport coefficients for use in the continuity and momentum equations are produced by stationary solutions of Boltzmann's equation for the electron energy distribution. Transport of secondary electrons emitted from surfaces is addressed using a Monte Carlo simulation.

To insure that there are no systematic changes in results using different algorithms with and without magnetic fields, the $B = 0$ cases discussed below actually use $B = 10^{-10}$ G with the same algorithms as a finite magnetic field. Tests were performed to confirm that results for $B = 10^{-10}$ G with magnetic field compliant algorithms gave essentially the same answer as $B = 0$ without magnetic field compliant algorithms. The reaction mechanism for Ar and Ar/Cl_2 mixtures is essentially the same as that described in [22] for Ar and [23] for Ar/Cl_2. The secondary electron emission coefficient was 0.1 for the top and bottom electrodes, 0.1 for the Si focus ring, 0.01 for the quartz focus ring, 0.05 for the metal surfaces surrounding the top electrode, and 0.03 for the metal sidewalls of the reactor. The secondary electron emission coefficient was zero on the pump face.

The algorithms for anomalous diffusion of electrons have been updated from the prior description of the model [21]. Anomalous diffusion refers to transport of charged particles perpendicular to magnetic field lines at a more rapid rate than given by classical expressions [24, 25]. In fluid simulations, transport perpendicular to magnetic field lines is often expressed as,

$$\mu_\perp = \frac{\mu_0}{\left(1 + \left(\frac{\omega_c}{\nu_m + \nu_a}\right)^2\right)}, \quad \omega_c = \frac{qB}{m} \tag{1}$$

where $\mu_\perp$ is the electron mobility perpendicular to the magnetic field (B-field) line, μ_o is the isotropic mobility, and ω_c is the cyclotron frequency for electron charge q and mass m in a magnetic field having magnitude B [26]. ν_m is the electron momentum transfer collision frequency and ν_a is the anomalous enhancement to that collision frequency. Given the dynamic, non-quiescent environment of an radio-frequency (RF) biased MERIE reactor, we expect there to be a significant anomalous component to the bulk transport. In this regard, we used

$$\nu_a = \alpha \nu_B \cdot \min\left(\frac{n_e}{n_0}, 1\right), \quad \nu_B = \frac{\omega_c}{16} \tag{2}$$

where ν_B is the Bohm anomalous collision frequency and α is a scaling factor [27]. The minimum function is in acknowledgement that the plasma within a MERIE is localized between the electrodes with spatial gradients in electron density, from as low as 10^5 cm^{-3} in the outer regions of the reactor to 10^{11} cm^{-3} between the electrodes. The source of anomalous diffusion, though certainly a topic of discussion, must scale with plasma density. A single isolated electron in cyclotron motion around a magnetic field line likely does not experience anomalous diffusion. n_0 represents a threshold electron density above which anomalous processes are important.

In the eMCS, the trajectories of individual electron pseudoparticles are integrated in time with collisions being accounted for using Monte Carlo techniques. Individual electron pseudoparticles undergo cyclotron motion perpendicular about the local B-field as a natural consequence of integrating their equations of motion. When an electron collision occurs with an atom or molecule, the electron is scattered isotropically (or anisotropically depending on the specific collision and energy) based on its instantaneous velocity. Following Bultinck *et al* [27], an anomalous collision frequency (equation (2)) was added to the energetically possible collisions an electron can undergo. In this regard, ν_a was added to the total collision frequency used to determine the time between collisions and in determining the null-collision frequency. If the anomalous collision is selected as the real collision, the velocity components in

the plane perpendicular to the local B-field were randomized, simulating an isotropic collision enhancing transport perpendicular to the B-field.

In the work discussed here, we used a collision frequency corresponding to full Bohm diffusion ($\alpha = 1$) and a threshold for the onset of anomalous effects of $n_0 = 1 \times 10^9$ cm^{-3}. The results here are not terribly sensitive to the choice of n_0 as the electron density in the bulk plasma exceeds 10^{11} cm^{-3} with gradients at the edges of the bulk plasma [10^{11} cm^{-3}]/cm. As long as n_0 is smaller than the average density in the bulk plasma (which prior studies suggest), the transition between the anomalous and non-anomalous regimes shifts laterally in the reactor by at best a cm. The sensitivity of the results of this investigation to the value of α is discussed in section 3.3.

3. Plasma properties with tilted magnetic fields

The system used for this study is a single frequency, 10 MHz CCP having an externally applied magnetic field nominally parallel to the bottom powered electrode. The geometry used in this investigation is shown in figure 1. In order to address misalignment in the magnetic field, the calculation was performed in a Cartesian coordinate system for a wafer that is 20 cm wide. The depth used for calculation of power deposition and gas flow rates was chosen to give a wafer area equivalent to a 20 cm diameter wafer. Power is applied to the substrate through an electrode in contact with the wafer, with the electrical feed to the electrode embedded in a dielectric chuck having relative permittivity equal to that of Teflon, $\varepsilon_r = 2$. The wafer is surrounded by a silicon annulus 3.1 cm wide under which the electrode extends. The Teflon chuck is surrounded by a quartz ring 4 cm wide. The sidewalls and top surface of the reactor are grounded metal. The metal showerhead is 34 cm widel. The wafer to showerhead gap is 2.5 cm. The actual aspect ratio of the reactor is shown in the upper image of figure 1. All other figures will use the layout shown in the lower image of figure 1 where the scale for the vertical direction has been expanded by a factor of 1.5 to enable more detail in the gap to be viewed. The numerical mesh is 256 cells wide and 60 cells high, for a cell size of 1.6 mm wide × 0.8 mm tall.

3.1. Plasma properties for magnetically enhanced Ar CCPs

As a reference case, plasma properties for the CCP sustained in Ar at 40 mTorr with 200 W power deposition and $B = 0$ are shown in figure 2. The ion density is maximum near mid-gap at 3.8×10^{10} cm^{-3}, and is uniform within 2%–3% over the width of the wafer. There is a local maximum of 4×10^{10} cm^{-3} above the focus ring due to electric field enhancement at the intersection of the Si and quartz rings. The electron temperature T_e is uniform across the wafer with a value of 4.5 eV, with there again being a small maximum above the focus rings of 4.6 eV. The nearly uniform electron temperature is due to the high isotropic thermal conductivity. The electron impact ionization source due to bulk electrons, S_e, is similarly uniform above the wafer with a value of 5.8×10^{15} cm^{-3}s^{-1} at mid-gap above the wafer. The electron impact ionization source due to secondary electrons emitted from all surfaces accounts for about 10% of the total ionization. The RF voltage amplitude to deliver 200 W is 101 V. With the top-bottom symmetry of this reactor being fairly good, the self-generated DC bias is only −4 V. The RF cycle averaged electric potential, uniform across the wafer, is maximum at mid-gap with a value of 43 V.

Plasma properties are shown in figure 3 for the same operating conditions (Ar, 200 W, 10 MHz, 40 mTorr) with a uniform static magnetic field of $B = 100$ G oriented parallel to the electrodes. For these conditions, the electron Hall factor (ω_c/ν_m, electron cyclotron frequency/momentum transfer collision frequency) is about 10 whereas that for the ions is 0.005. With the electrons being magnetized and the ions not being magnetized, there is moderate confinement that increases the ion density by a factor of 2.5 to 1.0×10^{11} cm^{-3} relative to the $B = 0$ case. The ion density decreases in uniformity parallel to the electrodes relative to the $B = 0$ case, taking on a diffusion dominated profile in the direction parallel to the B-field. The voltage amplitude required to deliver 200 W is 176 V with a DC bias of −8 V compared to 101 V for the $B = 0$ case. In spite of the higher electron density, the reduced cross-field mobility (in the axial direction) results in a higher resistivity needing a larger voltage amplitude to deliver 200 W.

With sheath oscillation being the dominant form of electron heating, T_e peaks at 5.7 eV in a few mm layer at the sheath edge above the wafer. With the transverse (axial) thermal conductivity being small due to magnetization of the electrons, the conduction (and convection) of this energy into the bulk plasma is small. Due to the high parallel thermal conductivity along the magnetic field lines, the high temperature electrons spread to the edge of the focus ring. The electron impact ionization source by bulk electrons, S_e, is similarly maximum at the lower sheath edge due to the local sheath heating. The electron impact ionization source by secondary electrons, S_{eb}, is confined within a few mm of the top

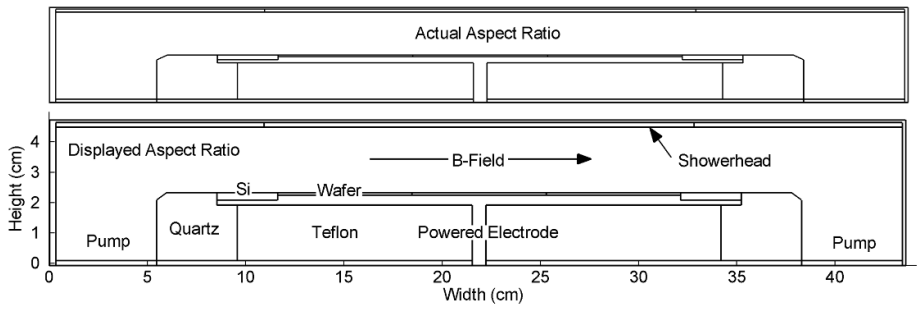


Figure 1. Schematic of the 2-dimensional Cartesian geometry. The substrate is powered at 10 MHz. A 20 cm wide wafer sits on the electrode surrounded by a Si annulus and quartz focus ring. The top image is the actual 1:1 aspect ratio of the reactor. The lower image is expanded in height (1:1.5) to enable detail to be seen.

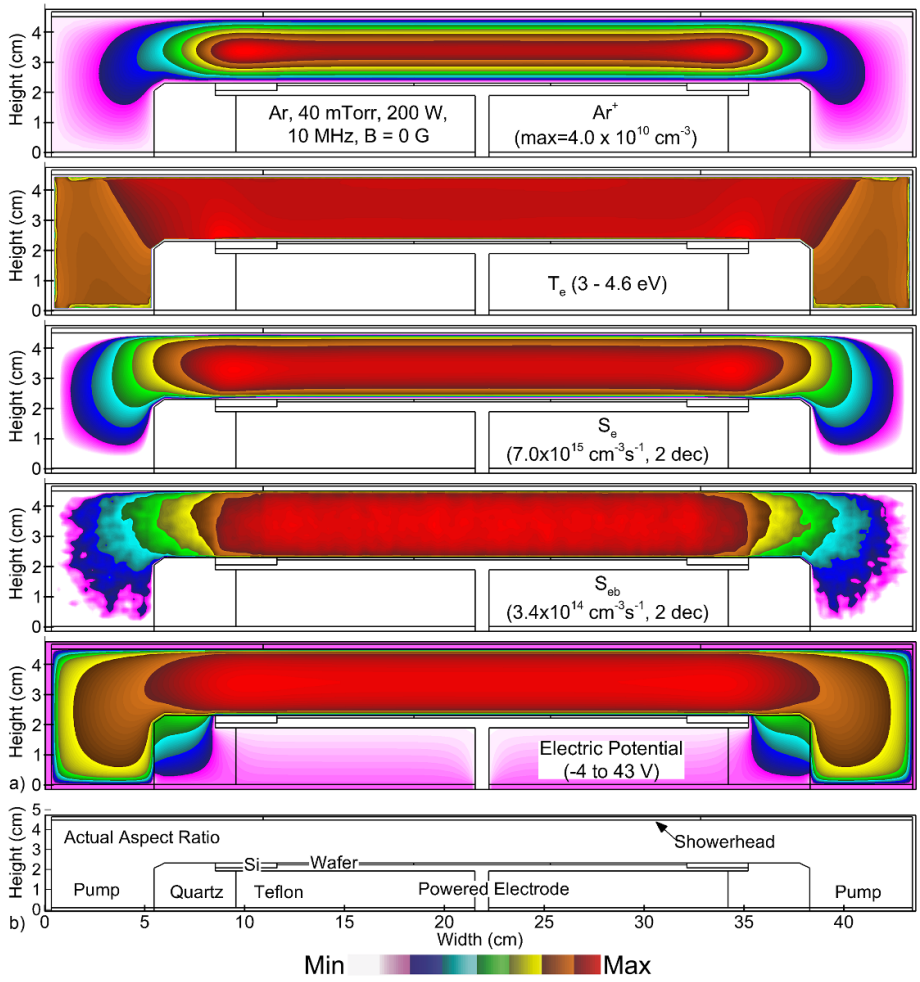


Figure 2. Plasma properties for the CCP sustained in Ar (40 mTorr, 10 MHz, 200 W) without a magnetic field. (a) (top to bottom) Ar^+ density, T_e (electron temperature), S_b (electron impact ionization by bulk electrons), S_{eb} (electron impact ionization by sheath accelerated secondary electrons and cycle averaged electric potential. The vertical scale of these images has been expanded by 1.5 to enable detail to be seen. The maximum or range of values is noted in each image. '2-dec' indicates a 2-decade logscale plot. (b) Schematic of the 2-dimensional Cartesian geometry with the actual aspect ratio.

and bottom surfaces, as secondary electrons emitted from those surface are confined by the parallel magnetic field.

Ion density is shown in figure 4 for 200 W for parallel magnetic fields of $B = 0$ G to $B = 150$ G. The Ar^+ fluxes to the wafer are shown in figure 5(a) for this range of magnetic field. With increasing confinement of electrons with increasing magnetic field, electron impact ionization sources transition to being closer to the substrate. The maximum ion density also moves to being lower in the reactor from

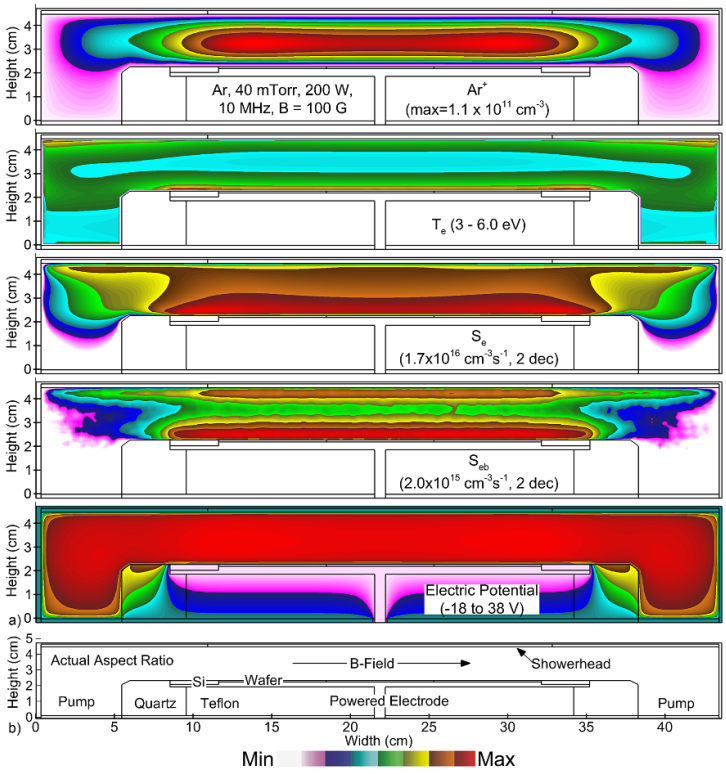


Figure 3. Plasma properties for the CCP sustained in Ar (40 mTorr, 10 MHz, 200 W) with a 100 G magnetic field parallel to the electrodes. (a) (top to bottom) Ar^+ density, T_e (electron temperature), S_b (electron impact ionization by bulk electrons), S_{eb} (electron impact ionization by sheath accelerated secondary electrons) and cycle averaged electric potential. The vertical scale of these images has been expanded by 1.5 to enable detail to be seen. The maximum or range of values is noted in each image. '2-dec' indicates a 2-decade logscale plot. (b) Schematic of the 2-dimensional Cartesian geometry with the actual aspect ratio.

mid-gap (1.2 cm above the wafer) with $B = 0$ G to 0.9 cm above the wafer for $B = 150$ G. The maximum ion density increases from 3.9×10^{10} cm^{-3} for $B = 0$ G to 1.4×10^{11} cm^{-3} for $B = 100$–125 G, which is also accompanied by an improvement in the uniformity in the ion flux to the substrate. Above 125 G, the ion density (and ion flux) transitions back to being edge high. It is at this magnetic field that hot electron transport parallel to the magnetic field disperses the ionization sources that would otherwise be centered over the wafer (as shown in figure 2). Although the maximum ion density decreases to 1.37×10^{11} cm^{-3} at $B = 150$ G, the total ion inventory (volume integral of ion density) continues to increase due to the lateral spreading of the plasma. The voltage required to deliver 200 W increases from 101 V ($V_{DC} = -4$ V) for $B = 0$ to a maximum of 180 V ($V_{DC} = -17$ V) for $B = 75$ G. The discharge becomes more asymmetric, though not dramatically so, with increase of magnetic field, indicated by the more negative DC bias as ionization occurs closer to the powered electrode.

Maintaining all conditions the same (200 W, 10 MHz, 40 mTorr), the $B = 100$ G magnetic field was tilted in angle with respect to the wafer, from 0° to 6.25°, slanting from low on the left side of the reactor to high on the right side. The resulting ion densities are shown in figure 6. The ion fluxes to the wafer for the 100 G magnetic field oriented at these angles are shown in figure 5(b). For tilt angles as small as 1°, there is an onset of side-to-side asymmetry in the ion density. The plasma density in the portion of the reactor beyond the limits of the powered electrode shows the greatest asymmetry. The side-to-side asymmetry in ion flux onto the wafer for a tilt of 1° is about 5%. For these conditions (100 G, 40 mTorr), the ion momentum transfer collision frequency is 7.3×10^5 s^{-1} whereas the ion cyclotron frequency is 3.8×10^3 s^{-1}, and so this nonuniformity is likely not the result of ion confinement. The electron impact ionization sources for this tilt do not show a significant side-to-side asymmetry. This first vestige of asymmetry results from parallel transport of relatively cool electrons along the magnetic field lines (down towards the left, up towards the right) which produces asymmetries in the cycle-averaged ambipolar electric fields. With tilt of the magnetic field, the voltage required to deliver 200 W remains fairly constant, within 5 V of 180 V.

When increasing tilt of the B-field, up to 6.25°, the ion density and ion flux to the wafer become increasingly more asymmetric. For a magnetic field tilt of 6.25°, the side-to-side asymmetry in ion flux to the wafer is 40%. The ion density is highly skewed (down towards the left, up towards the right). At

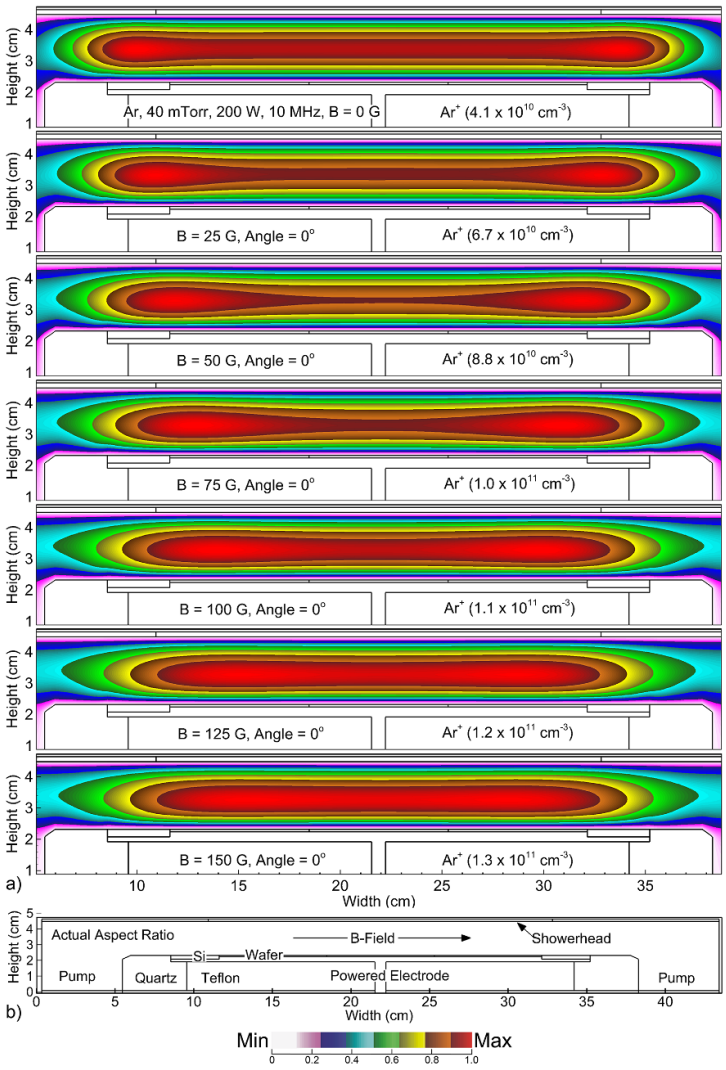


Figure 4. Ion density for the CCP sustained in Ar (40 mTorr, 10 MHz, 200 W). (a) (top to bottom) Magnetic fields from 0 to 150 G parallel to the electrodes with images expanded by 1.5 in the axial direction. The maximum value is noted in each image. (b) Schematic of the 2-dimensional Cartesian geometry with the actual aspect ratio.

this tilt angle the asymmetry in ion density and ion flux is due to several factors. The first is partly a consequence of the power being held constant with voltage being adjusted to deliver the specified power. Once the asymmetry occurs, there is higher plasma density skewed to the left which produces a local maximum in ion flux to the substrate Since the power is being held constant, there is positive feedback. The locally higher ion flux produces an increase in the local rate of ionization by secondary electrons confined by the magnetic field to the few mm near the substrate. With a fixed power, an increase in power in one region of the reactor decreases power in a different region by lowering voltage. The second factor is an EFR that, in spite of the apparent magnetization, produces vortexing and trapping of electrons during a portion of the cycle that accelerates electrons into the substrate to maintain charge neutral fluxes.

Simulations were performed for magnetic field angles of up to 10° and amplitudes of up to 150 G. The plasma could not be sustained between the electrodes for magnetic fields $>$ 100 G for angles $\geqslant$ 6.25°. Instead of the plasma being centered above the wafer, the centroid of the plasma was in the larger volume on the right side of the wafer above the pump ports. We have not pursued this avenue of research in detail as this inability to have a centrally located plasma is very geometry dependent. At these large angles and magnetic fields, electron transport along the magnetic field produces a high conductivity path from the powered electrode to the grounded electrode. This high conductivity path to some degree electrically shorts the sheaths, diminishing their ability to deposit power. As the voltage is adjusted to deliver the specified power, the more easily sustained plasma *off wafer* consumes that power, which results in little power left for the region between the electrodes.

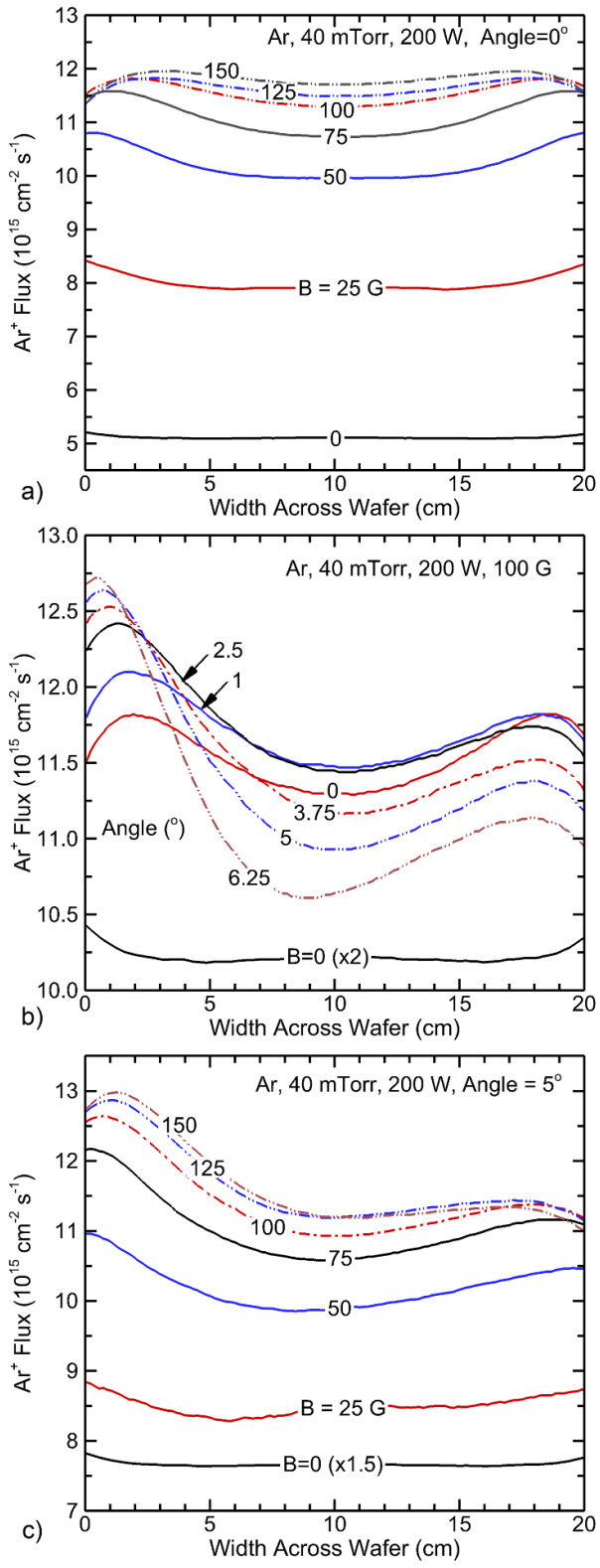


Figure 5. Ion flux onto the wafer for the CCP sustained in Ar (40 mTorr, 10 MHz, 200 W). (a) Magnetic fields of 0–150 G oriented parallel to the electrode. (b) Magnetic field of 100 G tilted at angles of 0–6.25°. (c) Magnetic fields of 0–150 G for a tilt angle of 5°.

The source of the asymmetries is, to first order, the magnetization of the electrons and their transport to align with the tilt of the magnetic fields. There is a secondary effect with respect to energy transport. The Ar^+ density, electron temperature, ionization sources and plasma potential are shown in figure 7 for a 150 G magnetic field tilted at 5°. Although there is a small asymmetry in the electron temperature at the sheath edge, a few tenths of an eV, there is not a sufficient change in electron

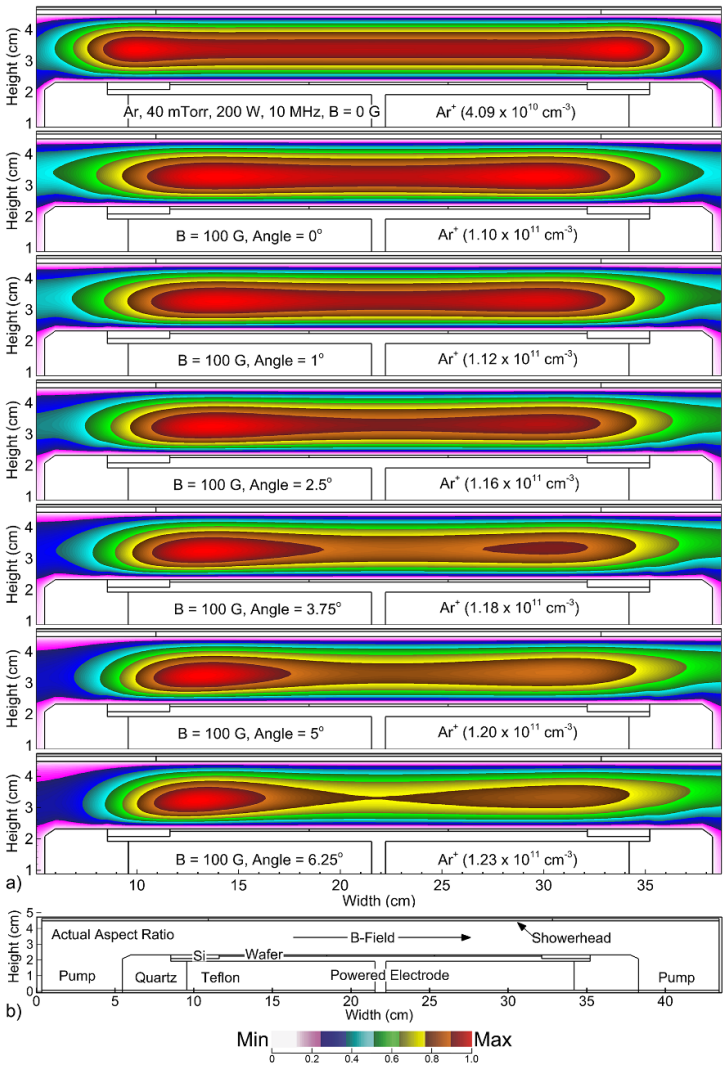


Figure 6. Ion density for the CCP sustained in Ar (40 mTorr, 10 MHz, 200 W) for a magnetic field of 100 G. (a) (top to bottom) Magnetic field tilted from 0 to 6.25° with images expanded by 1.5 in the axial direction. The ion density without a magnetic field is shown for comparison. The maximum value is noted in each image. (b) Schematic of the 2-dimensional Cartesian geometry with the actual aspect ratio.

impact rate coefficients to be solely responsible for the asymmetry in $Ar^{+\cdot}$ The asymmetry in the ionization source by bulk electrons is more a function of the change electron density due to transport than a change in rate coefficients. The same can be said for the ionization source by secondary electrons. The local increase in ion flux to the wafer generates more secondary electrons producing a larger local ionization source. These trends have the potential for being unstable due to the positive feedback mechanism mentioned earlier. Transport along the tilted magnetic field produces a local increase in plasma density whose larger flux to the wafer locally generates more ionization by secondary emission. There was less propensity for an instability in these simulations because the total power deposition was held constant. As current density increased, applied voltage decreased to maintain constant power. When applying a constant voltage with a low impedance power supply (no limit on current), the likelihood for an instability would be greater.

The asymmetry in plasma potential is to some degree a response to the asymmetry in plasma impedance. In the absence of the magnetic field, the majority of the current between the electrodes is purely axial. With a tilt in the magnetic field, some proportion of the current between the electrodes has a lateral component. With the plasma density shifted to the left, the left side of the reactor has a lower impedance than the right side. The response of the system is to increase potential on the right side to move current from right to left in the lateral direction.

When maintaining the tilt of the magnetic field at 5°, ion densities for magnetic field amplitudes of 0–150 G are shown in figure 8. Ion fluxes to the wafer for these conditions are shown in figure 5(c).

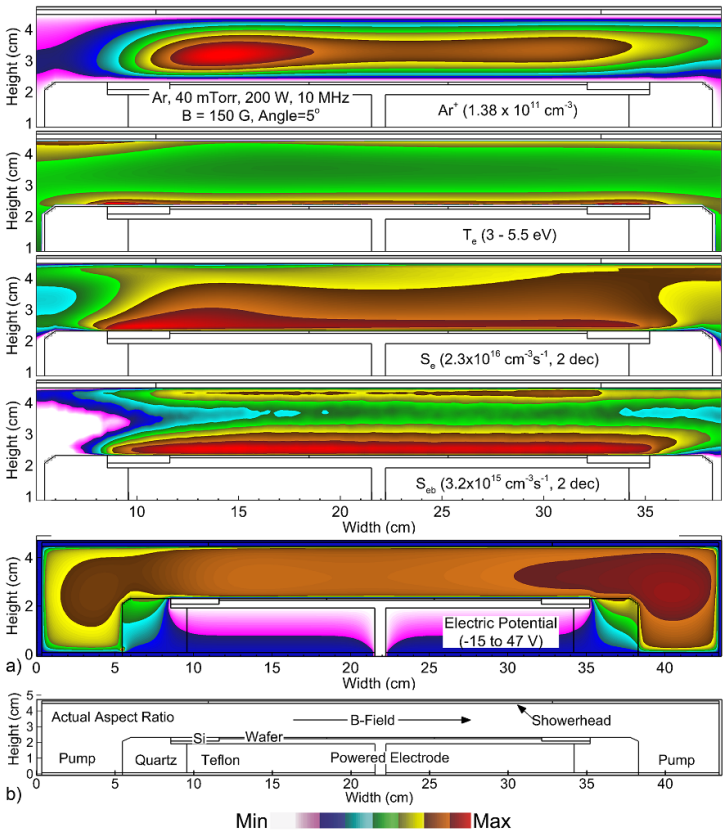


Figure 7. Plasma properties for the CCP sustained in Ar (40 mTorr, 10 MHz, 200 W) with a 150 G magnetic field tilted at 5°. (a) (top to bottom) Ar^+ density, T_e (electron temperature), S_b (electron impact ionization by bulk electrons), S_{eb} (electron impact ionization by sheath accelerated secondary electrons) and cycle averaged electric potential. The vertical scale of these images has been expanded by 1.5 to enable detail to be seen. The maximum or range of values is noted in each image. '2-dec' indicates a 2-decade logscale plot. (b) Schematic of the 2-dimensional Cartesian geometry with the actual aspect ratio.

The threshold for significant side-to-side asymmetries in ion flux for this tilt angle is 25–50 G. The fractional asymmetry over the wafer [$\delta = 2((\text{maximum flux})-(\text{minimum flux}))/(\text{maximum} + \text{minimum})$] increases from 1.2% to 15% for 0–150 G, while the integrated flux striking the wafer increases by a factor of 2.4.

Although ions are weakly magnetized for all values of magnetic field investigated here, the IEADs incident onto the wafer displayed side-to-side asymmetries. To investigate this scaling, the cycle averaged IEADs incident onto the left-, middle- and right-thirds of the wafer were collected. These distributions are shown in figure 9. The IEADs for $B = 0$ (figure 9(a)) are essentially uniform across the wafer, with an average energy of approximately half the RF amplitude. With a parallel magnetic field of B= 100 G, the IEADs across the wafer are also nearly uniform. With a larger voltage amplitude (176 V), the IEADs do extend to higher energies than the $B = 0$ case (101 V), however the increase is only moderate. With the magnetic field, the sheath is thicker and there is an EFR during the anodic portion of the cycle. In the thick sheath limit, ions average the potential during their transit time through the sheath which reduces the maximum ion energy. The EFR during a portion of the cycle reduces the ion energy overall. The small increase in maximum ion energy for the left and right portions of the wafer results from the increase in plasma density near the edge of the wafer relative to the $B = 0$ case, as shown in figure 4.

With a $B = 100$ G magnetic field tilted at 6.25°, the IEADs are non-uniform across the wafer, as shown in figure 9(c). The IEADs for the middle and right portion of the substrate are, nominally, the same. The IEAD on the left side is broader in energy. This extension in energy is due to a thinning of the sheath at that location as a result of the higher plasma density on the left side of the substrate and, generally, a higher plasma potential at the location. In the thin sheath limit, ions cross the sheath in a small fraction of the RF period, and so arrive at the substrate with nearly the instantaneous sheath potential. With the plasma being more conductive (higher electron density) at that location, there is a smaller voltage drop across the bulk plasma, leaving more voltage to be dropped across sheath, which then also contributes to the higher energy IEAD.

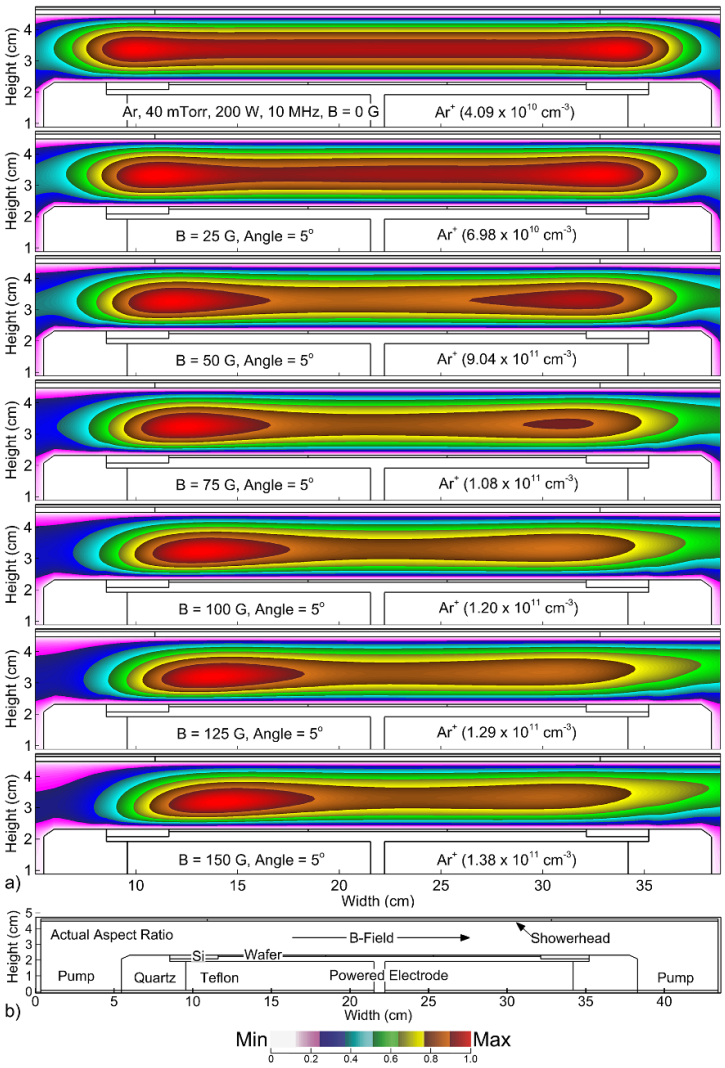


Figure 8. Ion density for the CCP sustained in Ar (40 mTorr, 10 MHz, 200 W) for a tilt angle of 5°. (a) (top to bottom) Magnetic fields of 0–150 G with images expanded by 1.5 in the axial direction. The maximum value is noted in each image. (b) Schematic of the 2-dimensional Cartesian geometry with the actual aspect ratio.

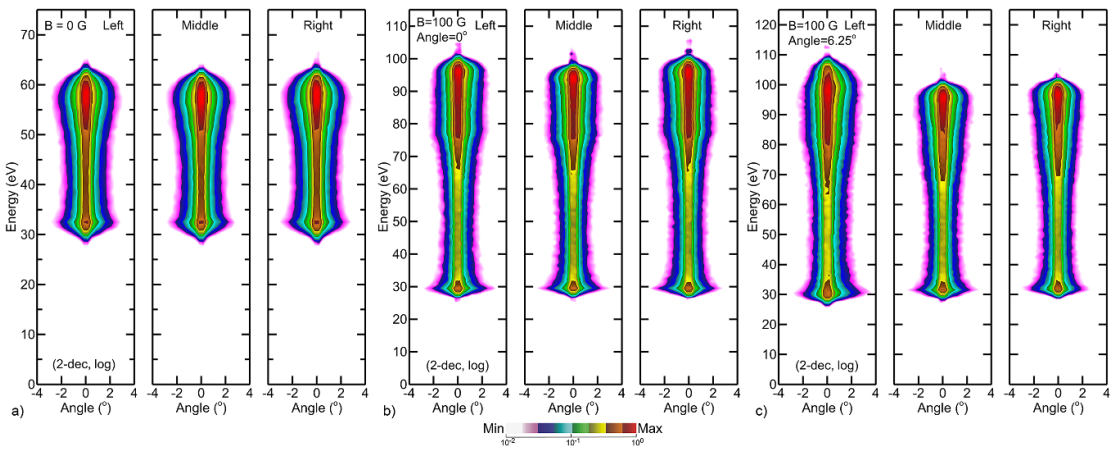


Figure 9. Ion energy and angular distributions (IEADs) to the wafer on the left, middle and right portions of the wafer for the CCP sustained in Ar (40 mTorr, 10 MHz, 200 W) (a) $B = 0$, (b) $B = 100$ G parallel to the electrodes and (c) $B = 100$ G with tilt angle of 6.25°. Images are plotted on a 2-decade log-scale.

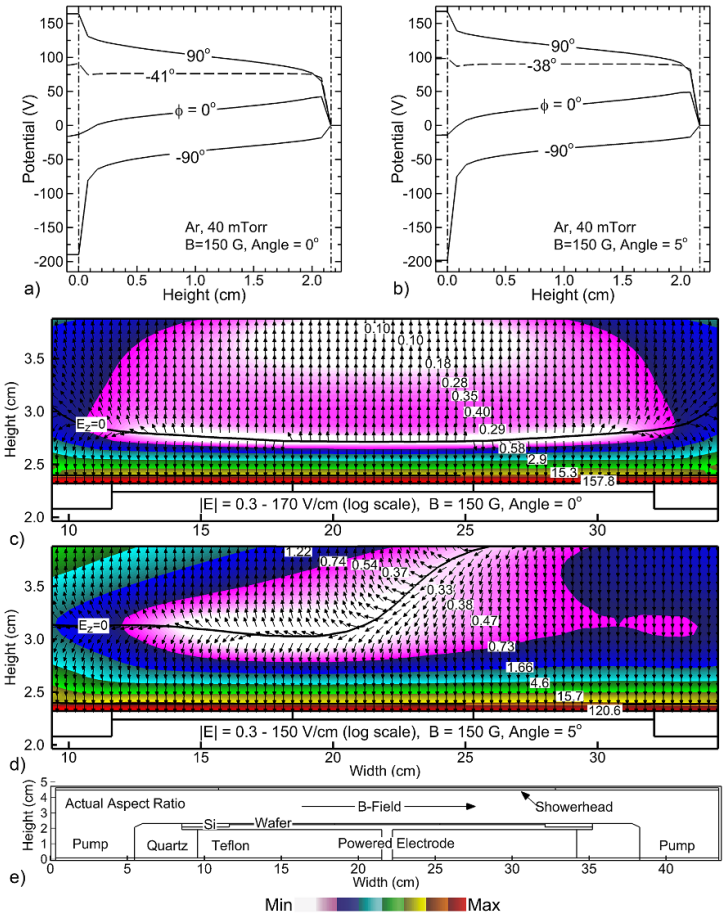


Figure 10. Electric potential and electric fields for Ar CCP (40 mTorr, 200 W) with a 150 G magnetic field and different tilt angles. Potentials as a function of height at the midplane at different phases during the RF cycle for (a) tilt = 0° and (b) tilt = 5°. The dashed line represents the *zero-crossing* phase for the axial electric field. Electric field (colour contours) and direction of electric field at the *zero crossing* phase for (c) tilt = 0° and (d) tilt = 5°. (e) Schematic of the 2-dimensional Cartesian geometry with the actual aspect ratio.

In the steady state and integrated over the RF cycle, the fluence (time integral of flux) of electrons and ions (negative and positive charge carriers) to the wafer must be the same. For sufficiently high frequencies, the ion flux into the wafer is essentially constant. Electrons flux to the wafer is confined to the peak of the anodic (most positive) portion of the RF cycle. Electron transport across the sheath to reach the wafer is usually dominated by diffusion. If the electron current due to the diffusion flux is insufficient to balance the positive ion current, negative charge accumulation in the presheath will produce an EFR. Instead of pointing towards the electrode (repelling electrons), the electric field momentarily points away from the electrode (attracting electrons). The EFR accelerates electrons into the powered electrode in order to balance ion current [20].

With magnetic fields parallel to the electrode, electron transport to the wafer is constrained, which then diminishes the ability of electron current to balance ion current. The response of the system is to produce an increasing more severe EFR to accelerate electrons across the magnetic field [11]. The plasma potential at mid-wafer as a function of height is shown in figure 10(a) for different phases during the RF cycle for a 150 G magnetic field parallel to the electrodes and in figure 10(b) for the magnetic field tilted at 5°. With mobility constrained electrons, there is a significant voltage drop across the bulk plasma to drive electron current to the top and bottom electrodes. At the peak of the anodic cycle (90°), the sheath is full reversed at the powered electrode. At the peak of the cathode cycle (−90°), the sheath is fully reversed at the grounded electrode. Qualitatively, the potential profiles are similar for the parallel and tilted magnetic fields, which there being a small phase change for the transition of the electric field in the bulk plasma from positive to negative.

The dynamics of the electric fields laterally across the wafer, however, are sensitive to the tilt angle of the electric fields. The electric fields in the vicinity of the lower electrode are shown in figure 10(c) for the 150 G magnetic field oriented parallel to the electrode, and in figure 10(d) for the magnetic field tilted at 5°. The RF phase of these images are when the axial electric field in the bulk plasma begins to

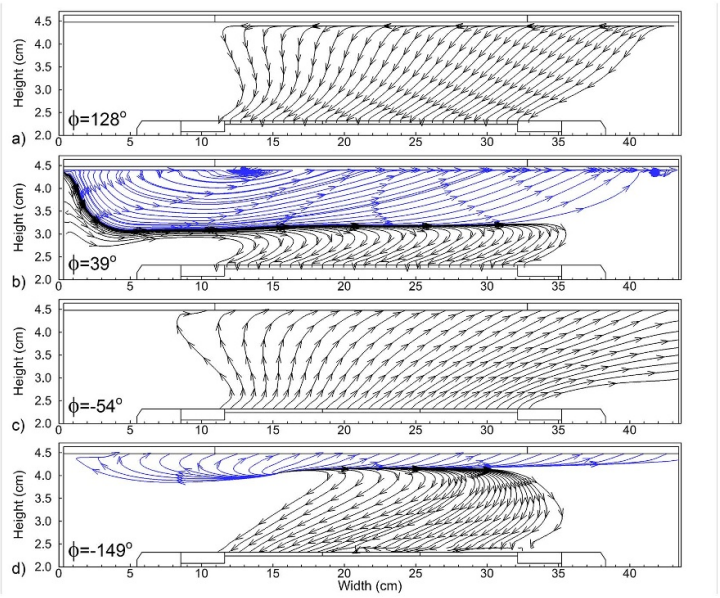


Figure 11. Streamlines for electron flux originating from (black) the lower electrode and (blue) from the upper electrode for Ar CCP (40 mTorr, 200 W) with a 150 G magnetic field with a tilt of 5°. Images are for different phases during the RF cycle (a) 128°, (b) 39°, (c) −54° and (d) −149°.

change from positive to negative, corresponding to the dotted lines in figures 10(a) and 10(b). The *zero-crossing* in axial electric field sweeps across the gap between the electrodes. With the magnetic field parallel to the electrodes, the *zero-crossing* sweeps vertically across the gap while remaining largely parallel to the electrodes. The small curvature in the *zero-crossing* is due to a thickening of the sheath over the focus rings at the edge of the wafer. With the 5° tilt in the magnetic field, the *zero-crossing* in the axial electric field sweeps across the reactor from bottom-right to top-left in a circuitous manner. This non-linear sweep of the *zero-crossing* is accompanied by (or caused by) vortices in the electron flux which also transitions from bottom right to upper left.

Although MERIE reactors are typically RF driven, the electric field in the sheath above the wafer has a DC component. This is particularly the case for an asymmetric system in which a large DC bias develops on the blocking capacitor. In Ganta *et al* [2], 2-dimensional particle-in-cell simulations were performed of an RF driven MERIE in which the magnetic field is perpendicular to the plane of interest. Given a quasi-DC component of the sheath electric and the orientation of the magnetic field, $E \times B$drift produced an off-axis shift in the centroid of the plasma. In the simulations here with the electric field and magnetic field in the same plane, $\vec{E} \times \vec{B}$ drift is perpendicular to the plane of interest, and does not introduce the asymmetries observed by Ganta *et al* [2].

However with tilt with the magnetic field, there are transients that produce vortex motion in electron flux that are not directly a consequence of $\vec{E} \times \vec{B}$ drift as described by Ganta *et al* [2]. This vortex motion occurs for heavily tilted magnetic fields and is associated with the electric field in the bulk plasma pointing in the opposite directions above and below the *zero-crossing*, alternating in direction on each half cycle. The sweep of the *zero-crossing* across the plasma (figure 10) produces momentary regions of negative space charge to which the electrons rapidly respond.

Streamlines for electron flux are shown in figure 11 at different phases during the RF cycle for a magnetic field of $B = 150$ G tilted at 5°. These phases were chosen to highlight specific behaviour and correspond approximately to the maximum positive and negative substrate voltages, and the *zero-crossings* in electric field. The black streamlines originate from or flow from the wafer on the powered (lower) electrode. The blue streamlines originate from or flow to the grounded (upper electrode). The RF impedance of the plasma facing surfaces of the lower electrode is smallest for the wafer and largest for the outer focus ring. These conditions result in the majority of current flowing to the lower electrode passing through the wafer.

At the anodic peak of the cycle (figure 11(a)) the top electrode is most negative and the bottom electrode is most positive. Electron flux streamlines generally flow top to bottom, while being redirected to align with the tilted magnetic field. Lack of full alignment of the electron flux with the magnetic field results from the finite collision frequency, real and anomalous. Electron flux originating near the left

side of top electrode quickly realigns with the magnetic field. However, magnetic field lines originating at these locations terminate on the lower electrode at sites having a large impedance, while ions trajectories are less affected. Negative space charge develops that redirects electron flux to the lower impedance electrode across the magnetic field. When approaching the lower electrode, the electron flux realigns with the magnetic field. The end result is the S-shaped path.

A similar sequence of events occurs for the cathodic peak of the cycle (figure 11(c)) when the top electrode is most positive and the lower electrode is most negative. Here, electron flux originating from the wafer will generally align with the magnetic field and flow to grounded surfaces. However electron flux originating from the left side of the wafer align with a magnetic field line whose path to ground is a large impedance. Negative space charge develops that redirects electron flux on to magnetic fields lines that have a lower impedance to ground. Again, the end result is the S-shaped path.

The intermediate phases (figure 11(b) and 11(d)) correspond approximately to the *zero-crossings* in electric field passing from the anodic-to-cathodic cycles (figure 11(b)) and the cathodic-to-anodic cycles (figure 11(d)). During these reversals, there is a node that crosses the reactor in which electron flux is directed in opposite directions. For example, for the cathodic-to-anodic transition (figure 11(d)) the *zero-crossing* propagates from the bottom electrode to the top electrode (at a tilt). Below the *zero-crossing*, the lower electrode appears in the new role of being anodic, and so electron fluxes are directed downwards. Above the *zero-crossing* the top electrode retains its role as being anodic, and so electron fluxes are directed upwards. This dichotomy is facilitated by negative space charge that somewhat aligns with the *zero-crossing*.

During the anodic-to cathodic transition (figure 11(b)) the *zero-crossing* propagates from the top electrode to the bottom electrode (at a tilt). Below the *zero-crossing*, the lower electrode retains its role as being anodic, and so electron fluxes are directed downwards. Above the *zero-crossing* largely retains is role as being anodic, and so electron fluxes are directed upwards. The exception is the left side of the top electrode which has already made the transition to being cathodic, with electron fluxes directed downwards. These trajectories are facilitated by negative space charge that again somewhat aligns with the *zero-crossing*. The electron flux originating from the grounded electrode (which includes the side wall) below the *zero-crossing* continue on a path towards the anodic appearing lower electrode. The electron flux originating from the grounded electrode above the *zero-crossing* is redirected towards the anodic top electrode.

3.2. Plasma properties for magnetically enhanced Ar/Cl_2 CCPs

Plasma etching, in practice, often uses complex gas mixtures including mixtures producing negative ions. The multicomponent gas mixtures can produce ions having different transport coefficients which may respond differently to the perturbation of the plasma by the tilt of the magnetic field. To investigate this possibility, simulations were performed for a $Ar/Cl_2 = 70/30$ gas mixture. All other conditions are the same as for the argon only cases. In this gas mixture, there is the possibility of 4 positive ions, Ar^+, Ar_2^+, Cl_2^+ and Cl^+, and 2 negative ions, Cl_2^- and Cl^-. Due to the low rate of 3-body reactions at 40 mTorr, the densities of Ar_2^+ and Cl_2^- are small and their roles in charge transport can be ignored for this discussion.

The total positive ion densities are shown in figure 12 for the Ar/Cl_2 mixture for $B = 0$ and $B = 100$ G for tilt angles of 0° to 6.25°. The overall trends in plasma uniformity are similar to the Ar only case. The ion density increases by about 30% with application of the parallel magnetic field, with the centroid of the plasma approaching the substrate where hot, sheath heated bulk electrons and secondary electrons are confined by the magnetic field. With increasing tilt of the magnetic field, the maximum in plasma density shifts towards the left side as with the argon only cases. However, the plasma in the Ar/Cl_2 mixture remains qualitatively more uniform than the Ar only plasma. The electronegativity (negative ion density/electron density) at mid-gap on the right side is 7.1 for $B = 0$, decreasing to 3.7 with $B = 100$ G.

Although not a focus of this investigation, the ion densities in Ar/Cl_2 mixtures have striation-like structures in the periphery of the reactor, shown most prominently in the $B = 0$ results of figure 12. These striations are nearly stationary during a single RF cycle but propagate outwards over many tens to hundreds of RF cycles. Stationary striations within the electrode gap are commonly observed in CCPs sustained in attaching gases such as CF_4. These striations are attributed, at least in part, to the oppositely directed motion of negative and positive ions, and temporal modulation of the ambipolar electric field during the RF cycle [28, 29]. The striations here are not formed in the electrode gap but rather in the periphery of the reactor, and are travelling waves as opposed to stationary. There certainly could be a

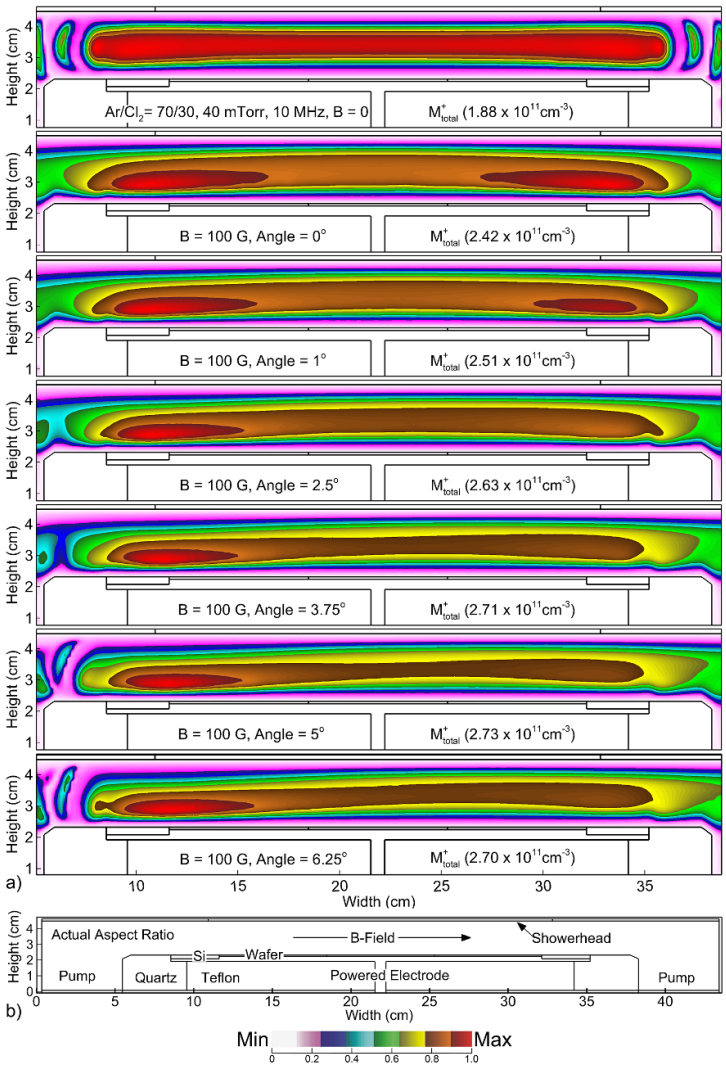


Figure 12. Total positive ion density for the CCP sustained in $Ar/Cl_2 = 70/30$ (40 mTorr, 10 MHz, 200 W) for a magnetic field of 100 G. (a) (top to bottom) Magnetic field tilted from 0 to 6.25°. with images expanded by 1.5 in the axial direction. The ion density without a magnetic field is shown for comparison at the top. The maximum value is noted in each image. (b) Schematic of the 2-dimensional Cartesian geometry with the actual aspect ratio.

contributing factor to the striations due to the spatial modulation in the ambipolar electric field as in the cited works, though the charge density associated with the striations in the periphery changes little during a single RF cycle. These structures are more likely the outcome of an ionization instability due to Cl_2 being a thermally attaching molecule whose rate coefficient for attachment increases with decreasing electron temperature. The electron temperature has a radial gradient (decreasing radially outwards) across the edge of the wafer and focus ring which modulates during the RF cycle. The net ionization rate (ionization minus attachment) then periodically transitions from positive to negative crossing over the edge of the wafer and focus ring. This modulation in net ionization then contributes to the striations.

The total ion flux to the wafer as a function of magnetic field for the Ar/Cl_2 mixture is shown in figure 13(a) for $B = 0$ and for $B = 100$ G for angular tilts of 0° to 7.5°. In the absence of a magnetic field, the ion flux is essentially uniform, having a non-uniformity of 2.7%. As with the Ar case, with increasing magnetic field, the ion flux is increasingly maximum on the left side of the wafer. The non-uniformity increases to 18% with a tilt of 5°, remaining at this non-uniformity through a tilt of 7.5°. Although these are significant non-uniformities, the positive ion fluxes for the electronegative mixture are less perturbed by the magnetic field than for the electropositive argon plasma. In electronegative Ar/Cl_2 plasmas, space charge is dominantly maintained by a balance between positive ions and Cl- negative ions, neither of which are magnetized for these conditions. Although the electrons are magnetized and non-uniform which produces an ionization source that is non-uniform, the resulting perturbation to

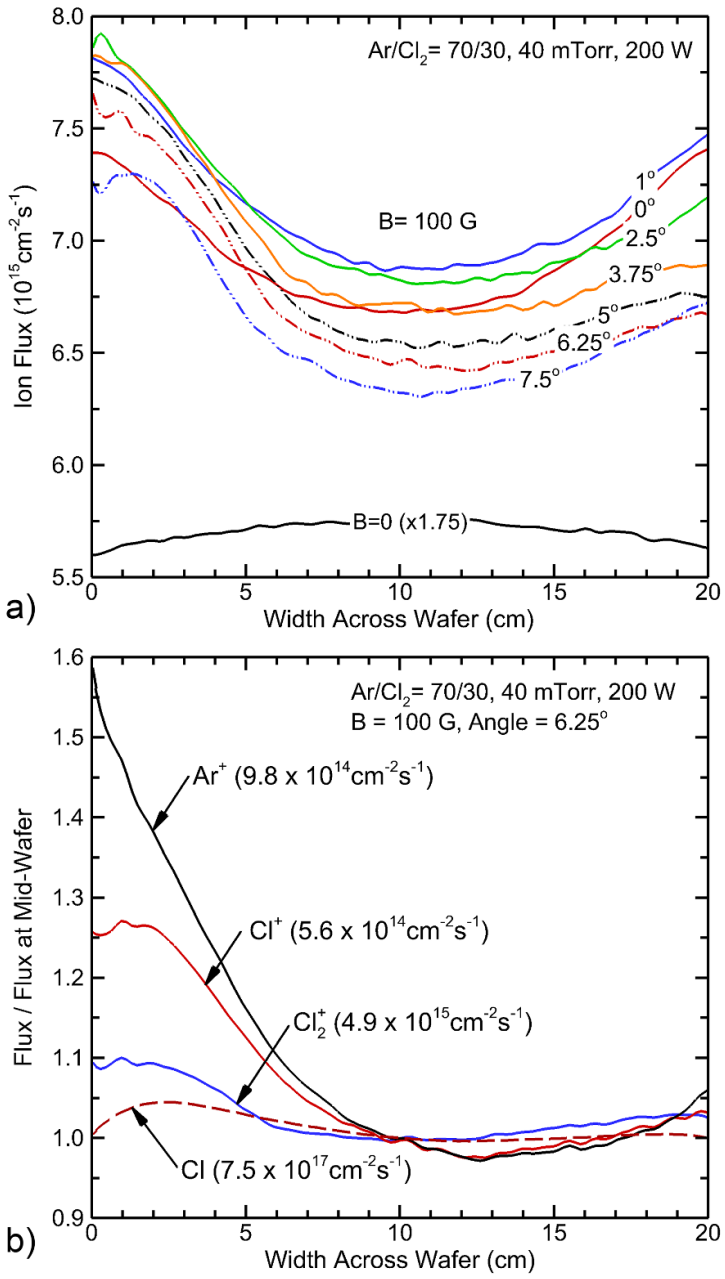


Figure 13. Positive ion flux onto the wafer for the CCP sustained in $Ar/Cl_2 = 70/30$ (40 mTorr, 10 MHz, 200 W) with a magnetic field of 100 G. (a) Total ion flux for tilt angles of 0–7.5°. Flux with $B = 0$ is shown for comparison. (b) Fluxes of individual ions and Cl atoms for a tilt angle of 6.25°. Fluxes are normalized by their value at mid-wafer.

the space charge is proportionately smaller due to the high electronegativity. The non-magnetized positive and negative ions are then able to maintain more diffusion dominated profiles.

For these conditions, the positive ion fluxes to the wafer dominantly consist of Ar^+, Cl_2^+ and Cl^+. Transport of each ion is in large part constrained by charge change. Ar^+ will charge exchange with all neutral species (including symmetric exchange with Ar). Cl^+ will charge exchange with Cl and Cl_2 (but not Ar). Cl_2^+ will only undergo symmetric charge exchange with Cl_2. The fluxes to the wafer for these three ions are shown in figure 13(b) for $B = 100$ G with a tilt of 6.25°. The uniformity of fluxes to the wafer differs for each ion, with the flux of Cl_2^+ being the most uniform and the flux of Ar^+ being the least uniform. These trends result in part from the locations where these ions are produced and their subsequent transport through the reactor. With Ar^+ having the largest ionization potential, its production is most sensitive to perturbations in electron temperature. With the maximum in T_e being skewed

to the left and towards the electrode due to the magnetic field, electron impact sources for Ar^+ are skewed to the left and compressed towards the electrode. With Ar^+ able to charge exchange to both Cl and Cl_2, its density is depleted when moving away from its site of formation. The end result is that the Ar^+ ion flux to the wafer largely reflects its location of formation.

At the other extreme, the ionization potential of Cl_2^+ is the smallest of the ions while Cl_2^+ is not depleted by charge exchange. As a consequence, the electron impact source for Cl_2^+ is more uniform across the reactor and, once generated, Cl_2^+ has a higher mobility and diffusivity. As a result, the flux of Cl_2^+ to the wafer is more uniform. Cl^+, with an intermediate ionization potential and ability to charge exchange with Cl_2 has a flux to the wafer that is more uniform than the flux of Ar^+ while being less uniform than the flux of Cl_2^+ to the wafer.

The flux of Cl atoms to the wafer is shown in figure 13(b), and shows little of the asymmetry of the ions. The transport of neutral Cl is not affected by the orientation of the magnetic field while the rates of gas phase reactions for Cl atoms are small at this pressure. The end result is that the Cl fluxes to the wafer are dominated by diffusion. The small asymmetry in the Cl flux is due to the skewing of the electron impact source function for Cl to the left by the tilt in the magnetic field.

3.3. Sensitivity to anomalous diffusion

The trends in MERIE plasma properties discussed to this point have used the anomalous diffusion model described in section 2 with an anomalous collision frequency corresponding to full Bohm diffusion. These trends are sensitive to the degree of anomalous diffusion, characterized by the fraction or multiplier of the Bohm anomalous collision frequency, α. This sensitivity is demonstrated by the ion densities shown in figure 14 and ion fluxes to the wafer shown in figure 15. These results are for the base case conditions (Ar, 40 mTorr, 200 W) with a 150 G magnetic field tilted at 5° while varying α from 0.1 to 10. At the lower range of α, cross field diffusion is dominated by the classical collision frequency. The distortion of ion density by alignment with the magnetic field is most severe. Ion flux to the wafer is correspondingly most severely shifted to the left. With increasing values of α, the anomalous collision frequency begins to dominate over the classical collision frequency, which then negates the distortion in ion densities and ion flux to the wafer produced by the tilted magnetic field. With $\alpha = 10$, the ion density and ion flux are essentially symmetric across the midplane of the reactor.

The increase in α produces a transition from cross field transport being dominated by the classical collision frequency to that being dominated by the anomalous collision frequency. During this transition, the maximum plasma density decreases from 2.1×10^{11} cm^{-3} (classical collision frequency) to 6.2×10^{10} cm^{-3} (dominated by anomalous diffusion) while the voltage required to deliver 200 W decreases from 183 V ($V_{DC} = -6.4$ V) to 138 V ($V_{DC} = -8.5$ V). In spite of the lower plasma density, the impedance of the plasma decreases with increasing α as indicated by the decrease in sustaining voltage. Even with the symmetry of the plasma and the apparent lack of influence of the magnetic field for $\alpha = 10$, the plasma density is still increased by 50% compared to the case with $B = 0$ (4.1×10^{10} cm^{-3}, figure 4(a)); and the voltage required to deliver 200 W is larger (138 V compared to 101 V) indicating a higher impedance plasma. This enhancement in density and increase in impedance results from the fact that even with a high anomalous collision frequency, electrons spend some small fraction of the RF cycle in cyclotron motion. This small fraction is sufficient to decrease their rate of cross field transport.

The characterization of anomalous transport here is the fraction (or multiplier) of Bohm diffusion, α, whose value has been applied uniformly across the plasma. The exception is the scaling of α with plasma density, equation (2), to acknowledge that a minimum plasma density is required to support anomalous processes. The value of α, or similar scaling parameters, can be functions of the local plasma properties, and of local turbulence in particular. The vortex motion of electron transport, discussed above, is not classical turbulence but likely does provide enough of a perturbation to increase anomalous electron transport. This increase in anomalous transport would have the effect of locally increasing α. Larger values of α lessen the consequences of tilt in the magnetic field. Given the likely sensitivity of α to local plasma conditions and to vortex motion (turbulence) in particular, having α be uniform across the plasma represents a worst case scenario for consequences of the tilt in the magnetic field.

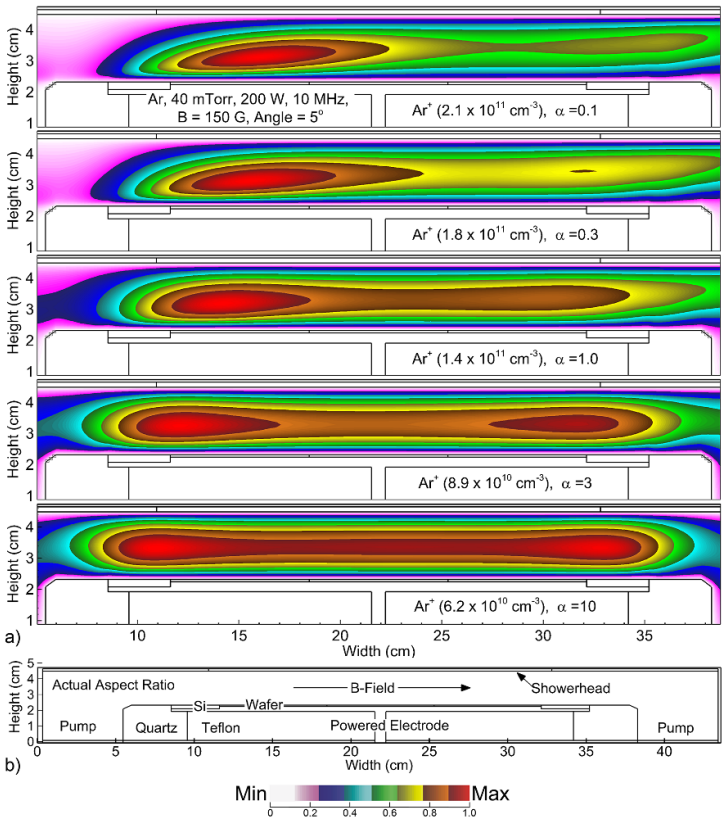


Figure 14. Total ion density for the CCP sustained in Ar (40 mTorr, 10 MHz, 200 W) for a magnetic field of 150 G tilted at 5° for different values of the anomalous diffusion parameter α. (a) (top to bottom) $\alpha = 0.1, 0.3, 1.0, 3, 10$, with images expanded by 1.5 in the axial direction. Maximum ion densities are noted in each frame. (b) Schematic of the 2-dimensional Cartesian geometry with the actual aspect ratio.

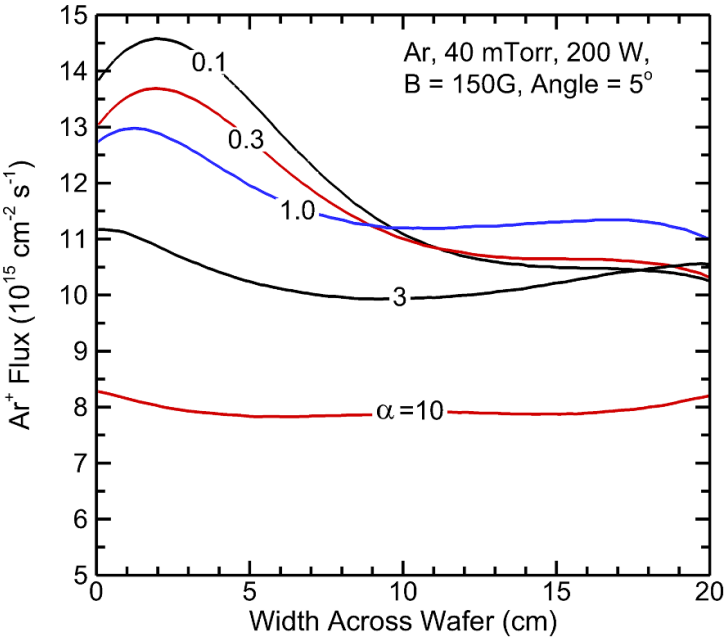


Figure 15. Ion flux onto the wafer for the CCP sustained in Ar (40 mTorr, 10 MHz, 200 W) with magnetic field of 150 G tilted at 5° for different values of the anomalous diffusion parameter α.

4. Concluding remarks

A computational investigation was conducted of the consequences of tilt of the magnetic field, nominally parallel to the substrate, in MERIE reactors - capactively coupled plasmas. The motivation for this study is to assess the reproducibility required in aligning the solenoids producing these magnetics after, for example, preventative maintenance of the plasma reactor. The test system was a CCP powered at 10 MHz sustained in Ar and Ar/Cl_2 mixtures at 40 mTorr and delivering 200 W to a 20 cm wide wafer. We found that tilts in the magnetic field as small as 1° produced significant non-uniformities in the distribution of plasma within the reactor and in ion fluxes incident onto the 20 cm wafer. The industry standard wafer is 30 cm in diameter. We expect that this sensitivity will scale with the size of the wafer with smaller tilts being more significant for larger wafers.

In the absence of a magnetic field, the ion flux to the wafer in the Ar CCP was symmetric side-to-side. For a magnetic field of 100 G, the side-to-side non-uniformity in ion fluxes produced by a 1° tilt was 5%. For a 6.25° tilt in magnetic field the non-uniformity was 40%. Larger magnetic fields and more severe tilts produced greater asymmetries in ion fluxes. The electric field reversals often observed in MERIE reactors are made more complex with the tilted magnetic fields with sweeping motions across the reactor. *Zero crossings* in the bulk electric field which are not parallel to the electrodes induce vortex-like motion of the electron fluxes.

These trends extended to Ar/Cl_2 mixtures with the added complication that the sensitivity of ion fluxes to the tilt in magnetic field is dependent on the transport properties of the individual ions. Fluxes to the wafer of ions having different ionization potentials and transport properties responded differently to the tilt in magnetic field. The flux of Ar^+ was most sensitive to the tilt in magnetic field as Ar^+ has the highest ionization potential and shortest mean free path for consumption. The flux of Cl_2^+ was least sensitive to the tilt in magnetic field as Cl_2^+ having the lowest ionization potential and longest mean free path for consumption.

These trends are sensitive to the anomalous diffusion model employed for electrons. The model employed here adds an anomalous collision frequency of $\nu_a = \alpha\nu_B, \quad \nu_B = \omega_c/16$. For the conditions of this study, $\alpha = 0.1$ produces the highest sensitivity to the tilted magnetic field with the largest asymmetry. $\alpha = 10$ produced an essentially symmetric plasma distribution, while still having a higher impedance than in the absence of a magnetic field. A detailed investigation of the source of anomalous diffusion is beyond the scope of this study. However, it is likely that anomalous diffusion is more prevalent at higher powers, lower pressures and in atom dominated gas mixtures.

The first order impact on plasma processing using a MERIE having a tilted magnetics field is the change in the uniformity of the ion fluxes incident onto the wafer which then impacts processing uniformity. The non-uniformity across the wafer of the incident ion energy distributions would likely be a lesser concern. The second order impact of the tilted magnetic field is due to the changes in the relative ratios of the fluxes of incident reactive species onto the wafer. In reactive, multi-component gas mixtures, the response to the tilted magnetic field can differ between different species. For example, the different responses of Ar^+, Cl^+ and Cl_2^+ to tilt in the magnetic field produced fluxes to the wafer with different spatial dependence, with all being different from the flux of Cl atoms. These spatially differing ratios of fluxes can then directly impact processing rates and selectivity.

The focus of this paper has been the possible detrimental consequences of tilted magnetic fields in MERIE-like systems in the context of semiconductor processing. At the same time, there are potential benefits from deliberately tilting magnetic fields in parallel plate CCPs. For example, Sun *et al* [30] describe a resonance mode in RF excited CCPs having tilted magnetic fields which enhances electron power deposition. In the context of plasma processing for semiconductor fabrication, there are at least two metrics to consider when evaluating the consequences of any modification to the system, including tilted magnetic fields. Those metrics are efficiency and uniformity. Efficiency refers to the ability to deposit power in the plasma to maximize production of the desired fluxes of electrons, ions, radicals and photons to the wafer. Uniformity refers to delivering those fluxes to the wafer (including their energy and angular distributions) with the minimum of variation. An often quoted metric in the semiconductor industry is that fluxes should be uniform to better than 1% across a 30 cm wafer. In the context of semiconductor manufacturing, evaluating the potential benefits of any modification or perturbation of the system should consider both of these metrics.

In this study, the magnetic fields are static (non-time varying) and, while being tilted, are spatially uniform. In commercial MERIE reactors, the magnetic fields are often produced by a set of solenoidal coils which are not spatially uniform. The magnetic fields are then rotated around the reactor (either by varying current in the solenoids or by physical rotation) with the goal of producing a time averaged

uniform magnetic field [7, 8]. The period of rotation is typically long compared to the plasma hydrodynamic timescales so that at any instant the magnetic field appears to be static. In this regard, the conclusions of this study with respect to misalignment are applicable to the instantaneous magnetic field configurations in a rotating system. Rotating the magnetic fields would likely average the consequences of misalignment if those misalignments are random amongst the individual solenoids. If, however, the misalignment is universal (i.e. all solenoids are titled in the same direction), then rotating the magnetic fields would likely be less successful in averaging the consequences of misalignment.

The development of digital twins (DTs) based on surrogate models (SMs) relies on the robustness and accuracy of the physics models which provide the needed training data. Given the challenges in the availability of fundamental data and reactions mechanisms for the physics models and the potentially vast parameter spaces needed to be surveyed, DTs based on *omni-surrogate-models* are still likely some time in the future. In the near term, DTs based on SMs may be best applied to problems which are more narrowly defined covering smaller parameter spaces and which depend on more dimensional variations as opposed to chemistry variations. An example of such a problem is restoring a plasma reactor to the same performance following dis-assembly and re-assembly during maintenance. The changes in reactor performance resulting from dimensional variations (such as orientation of the magnetic field) are less sensitive to subtleties due to changes in plasma chemistry that might be encountered in using SMs for process development.

Acknowledgment

This work was supported by Samsung Electronics Co., Ltd.

Data availability statement

The data supporting this work is contained within this paper or is available upon reasonable request from the authors.

Conflict of interest

The authors have no conflicts of interest to disclose.

ORCID iD

Mark J Kushner 0000-0001-7437-8573

References

[1] Oehrlein G S *et al* 2024 *J. Vac. Sci. Technol. B* **42** 041501
[2] Ganta S S, Bera K, Rauf S, Kaganovich I, Khrabrov A, Powis A T, Sydorenko D and Xu L 2024 *Phys. Plasmas* **31** 102107
[3] Sharma S, Patil S, Sengupta S, Sen A, Khrabrov A and Kaganovich I 2022 *Phys. Plasmas* **29** 063501
[4] Tsankov T V, Chabert P and Czarnetzki U 2022 *Plasma Sources Sci. Technol.* **31** 084007
[5] Zhang Q-Z, Liu J-R, Liu Y-X, Lu W-Q, Sun J-Y and Wang Y-N 2022 *Plasma Sources Sci. Technol.* **31** 07LT01
[6] Barnat E V, Miller P A and Paterson A M 2008 *Plasma Sources Sci. Technol.* **17** 045005
[7] Buie M J, Pender J T P and Dahimene M 1998 *J. Vac. Sci. Technol. A* **16** 1464
[8] Lindley R A, Bjorkman C H, Shan H, Ke K H, Doan K, Mett R R and Welch M 1998 *J. Vac. Sci. Technol. A* **16** 1600
[9] Lee S H, You S J, Y.chang H and Lee J K 2007 *J. Vac. Sci. Technol. A* **25** 455
[10] Kanarik K J, Tan S and Gottscho R A 2018 *J. Phys. Chem. Lett* **9** 4814
[11] Kushner M 2003 *J. Appl. Phys.* **94** 1436
[12] Dahiya S, Sharma N, Geete S, Sharma S, Sirse N and Karkari S 2024 *Phys. Plasmas* **31** 083512
[13] Jeong S-Y and Choi C H 2025 *Phys. Plasmas* **32** 123502
[14] Ko J, Bae J, Park M, Jo Y, Lee H, Kim K, Yoo S, Nam S K, Sung D and Kim B 2023 *J. Phys. D: Appl. Phys.* **56** 344001
[15] Filipovic L 2025 From atoms to reactors: multi-scale modeling for semiconductor fabrication *2025 Int. Conf. on Simulation of Semiconductor Processes and Devices (SISPAD)* pp 1–4
[16] Osborne G, Roy S, Webb E, McDevitt C J and Roy S 2026 *Phys. Fluids* **38** 037119
[17] Trieschmann J, Vialetto L and Gergs T 2023 *J. Micro/Nanopattern. Matls. Metrol.* **22** 041504
[18] Boniakou E *et al* 2026 A hybrid physics-machine learning framework for fast, predictive low-pressure plasma etching models *Proc. SPIE 13984, Advanced Etch Technology and Process Integration for Nanopatterning XV* 139840U
[19] Doyle S J, Larson A, Rosenzweig G, Gunn J and Kushner M J 2024 *J. Phys. D: Appl. Phys.* **57** 435202

[20] Krüger F, Lee H, Nam S K and Kushner M J 2024 *Phys. Plasmas* **31** 033508
[21] Song S-H, Yang Y, Chabert P and Kushner M J 2014 *Phys. Plasmas* **21** 093512
[22] Tian P and Kushner M J 2015 *Plasma Sources Sci. Technol.* **24** 034017
[23] Tian P and Kushner M J 2017 *Plasma Sources Sci. Technol.* **26** 024005
[24] Bradley J W, Thompson S and Gonzalvo Y A 2001 *Plasma Sources Sci. Technol.* **10** 490
[25] Andrews S, Andriulli R, Sourhair N, Magarotto M and Ponti F 2025 *Plasma Sources Sci. Technol.* **34** 065513
[26] Hagelaar G J M, Bareilles J, Garrigues L and Boeuf J-P 2002 *J. Appl. Phys.* **91** 5592
[27] Bultinck E, Mahieu S, Depla D and Bogaerts A 2010 *J. Phys. D: Appl. Phys.* **43** 292001
[28] Liu Y-X, Korolov I, Schüngel E, Wang Y-N, Donkó Z and Schulze J 2017 *Phys. Plasmas* **24** 073512
[29] Masheyeva R, Vass M, Wang X-K, Liu Y-X, Derzsi A, Hartmann P, Schulze J and Donkó Z 2024 *Plasma Sources Sci. Technol.* **33** 045019
[30] Sun J-Y, Gao F, Zhou F-J, Schulze J and Wang Y-N 2024 *Phys. Rev. Lett.* **133** 235302